

Self-Similar Spatiotemporal Structure of Intermaterial Boundaries in Chaotic Flows

M. M. Alvarez,¹ F. J. Muzzio,^{1,*} S. Cerbelli,¹ A. Adrover,² and M. Giona³

¹Department of Chemical and Biochemical Engineering, Rutgers University, Piscataway, New Jersey 08855

²Dipartimento di Ingegneria Chimica, Università di Roma "La Sapienza," Via Eudossiana 18, 00184 Roma, Italy

³Dipartimento di Ingegneria Chimica, Università di Cagliari, Piazza d'Armi, 09123 Cagliari, Italy

(Received 24 July 1997)

The evolution of macroscopic material closed filaments in a time-periodic chaotic 2D flow is simulated for cases with large, small, and very small islands of regular motion using an algorithm that preserves spatial continuity. The length of the stretched filament increases much faster than predicted by the Liapunov exponent. In chaotic regions, the filament asymptotically evolves into a self-similar structure with *permanent* spatial nonuniformities in density. Filament densities and local length scales corresponding to different times are described by families of frequency distributions with invariant shape that can be collapsed onto a single curve by means of a simple scaling. [S0031-9007(98)07190-7]

PACS numbers: 47.52.+j, 47.11.+j, 47.53.+n

This paper focuses on the time evolution of spatial structures generated by mixing in chaotic flows. Experiments [1–4] and computations (Fig. 1) have revealed that such structures are composed of thousands of thin striations with an overall pattern that remains invariant over time. The length scale distribution of such structures is of considerable importance. For example, in polymer blends, it determines mechanical and optical properties. In transport-controlled reactive systems, microstructure determines both the overall rate of reaction [5] and the relative amounts of different products generated by the process [5]. In magnetic dynamos, microstructure determines the spatial distribution of magnetic intensities [6–9].

The rate of decay of length scales, the spatial density of material lines, and the length scale distribution of partially mixed structures generated by chaotic flows have never been characterized in detail, either in real or in model flows. Chaotic flows create structures with a wide distribution of length scales, most of which are beyond experimental resolution. Most previous mixing studies have focused on advection of point tracers [10,11] or stretching of infinitesimal vectors [12,13]. Such simulations cannot be used to examine the length scale distribution of a partially mixed structure. Evolution of material filaments in chaotic flows was originally considered by Franjione *et al.* [14], who concluded that the large computational resources required to simulate the exponentially growing filament made such quantifications impractical at the time. Fung and Vassilicos [15] attempted an analysis of convected filaments, but their algorithm failed to preserve continuity along the lines. Beigie *et al.* [12], Ziemniak *et al.* [16], and Neufeld and Tél [17] preserved the continuity of the filament, but did not examine the topology of the structures generated by the flow.

The evolution of material lines has also been considered in studies dealing with kinematic dynamos in infinitely conducting fluids [6–9], which is closely related to the problem studied here: Both systems evolve as predicted

by the convection-stretching equation,

$$D\partial x/Dt = \partial x \cdot \nabla u, \quad DB/Dt = \mathbf{B} \cdot \nabla u, \quad (1)$$

where u is the velocity field, ∂x is an infinitesimal element of a material line, and \mathbf{B} is the magnetic field. However, the two problems are different in several important

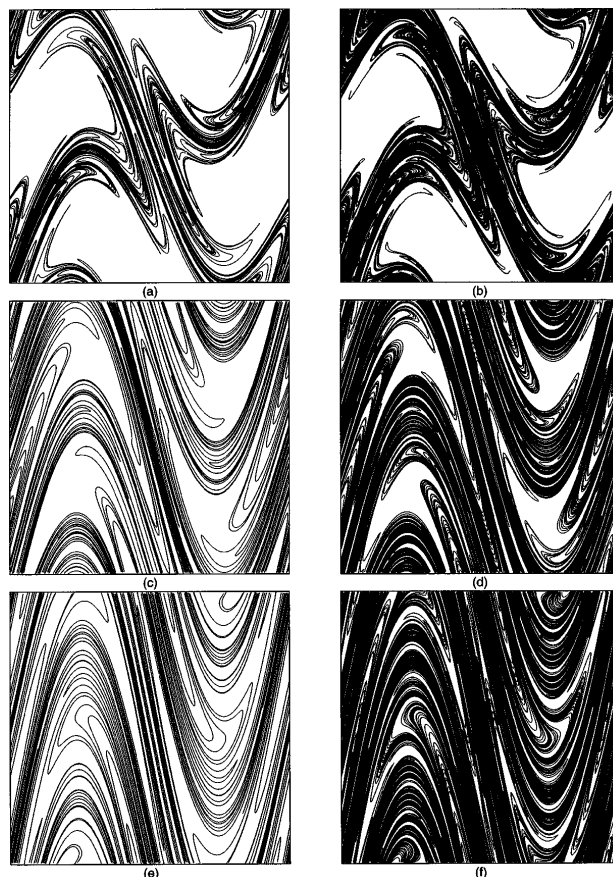


FIG. 1. Evolution of a material filament in the sine flow: (a) $T = 0.8, n = 8$; (b) $T = 0.8, n = 10$; (c) $T = 1.2, n = 5$; (d) $T = 1.2, n = 6$; (e) $T = 1.6, n = 4$; (f) $T = 1.6, n = 5$.

respects. While fast dynamos cannot exist in 2D continuous flows, mixing of chemical species can occur in the time-periodic 2D flows studied here. In 3D, while magnetic fields evolve via line stretching, reactive mixing is directly dependent on surface stretching. Finally, while the uncoupling between \mathbf{B} and \mathbf{v} in magnetic fields is a (somewhat restricting) simplification, in scalar mixing the material lines rarely affect the velocity field.

In this paper, the evolution of fluid material lines is analyzed by following the deformation of continuous closed filaments as they are stretched, advected, and folded by the time-periodic chaotic sine flow [18], which is defined in the infinite domain by the two motions:

$$(V_x, V_y) = (\sin 2\pi y, 0), \quad nT \leq t < (n + \frac{1}{2})T, \quad (2a)$$

$$(V_x, V_y) = (0, \sin 2\pi x), \quad (n + \frac{1}{2})T \leq t < (n + 1)T, \quad (2b)$$

where T is the flow period, n is the number of periods, and t is time. This model flow is continuous and differentiable to any order, including at the boundaries (when defined only in a unitary box). The sine flow is useful and relevant for two main reasons: (1) Its simplicity makes it possible to gather large amounts of information at a moderate computational cost, and (2) it generates stretching and curvature distributions that are essentially identical to those observed in industrial flow systems [19].

Filaments are initially represented using closed circular strings of uniformly spaced points centered at $(0.5, 0.5)$ with radius $r = 0.01$. Subsequently, the algorithm finds the positions of the points after the first motion period. The distances between consecutive points are calculated; whenever two points move apart more than a distance d , new points are interpolated *along the arc of the original filament*, renumbered to preserve order and continuity, and mapped to find their convected position. The algorithm is then iterated for successive periods, always performing the addition of points along the original curve. Figures 1(a) and 1(b) show filaments for the case $T = 0.8$ (a partially chaotic condition characterized by four large period-2 regular islands and many small ones) for 8 and 10 periods of the flow, respectively. The value of $d = 0.01$ was adopted for this computation, and periodic boundary conditions were imposed such that the flow map operates in a unitary domain (analogous to a toroidal surface). A complex structure emerges after just a few periods, which, as expected from previous experimental and numerical work [4,13,19], displays strong symptoms of self-similarity. As time increases, the process preserves all features generated in earlier work flow periods, adding new details within and around previously existing ones. Results for $T = 1.2, n = 5$ and 6 periods are shown in Figs. 1(c) and 1(d), respectively. The flow is mainly chaotic at this value of T . As before, the filament grows very fast, generating a structure that is evidently

self-similar in time. Finally, Figs. 1(e) and 1(f) shows the filament obtained for $T = 1.6, n = 4$ and 5 periods. For this “globally chaotic” case, the self-similar structure quickly invades almost all of the flow domain.

For this flow condition, a Poincaré section would be nearly featureless, and would look like a random cloud of points, suggesting that a globally chaotic flow would eventually generate a completely homogeneous system. However, actual mixing behavior is more complex. A very wide distribution of local length scales and filament densities is apparent in Fig. 1. This observation is made explicit by calculating the filament density ρ , which is computed by dividing the flow domain into equal-sized boxes and calculating the length of the filament contained in each box divided by the area of the box. Such computation reveals that values of ρ span several orders of magnitude (Fig. 2), which means that in some regions the flow achieves much more intimate mixing of components than in other regions. Regions of high density correspond to regions of fast stretching [18,19]. Figure 3 (main panel) shows the frequency distribution of filament densities, $F_n(\rho) = (1/N_\rho)dN(\rho)/d\rho$ (where N_ρ is the total number of boxes and $dN(\rho)$ is the number of boxes with densities between ρ and $\rho + d\rho$). Distributions corresponding to different flow periods have identical shapes and are collapsed onto a single curve by a simple scaling $\Gamma(v) = \langle \rho \rangle F_n(\rho)$; $v = \rho / \langle \rho \rangle$, where $\langle \rho \rangle$ is the average density. The collapse of $\Gamma(v)$ over several orders of magnitude in $F_n(\rho)$ and ρ suggests that such nonuniformities in filament density are a *permanent* feature of time-periodic chaotic flows.

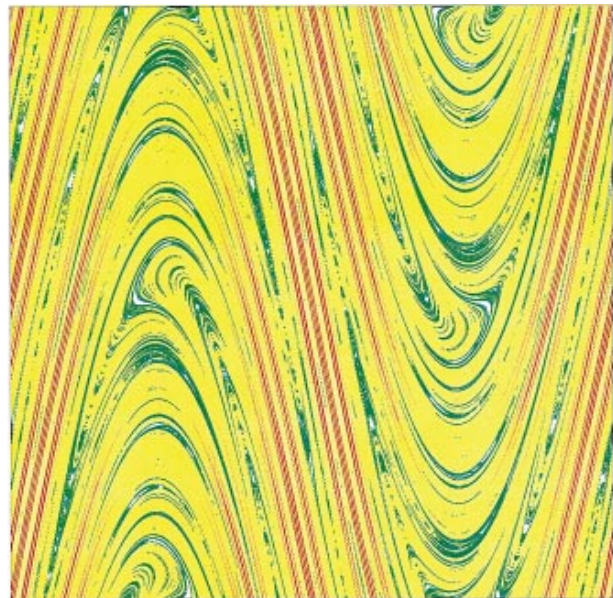


FIG. 2(color). Density ρ for $T = 1.6, n = 7$. Colors are assigned *ad hoc*: red: $1.5 \geq \log(\rho/\langle \rho \rangle) \geq 0.5$; yellow: $0.5 > \log(\rho/\langle \rho \rangle) \geq -0.5$; green: $-0.5 > \log(\rho/\langle \rho \rangle) \geq -1.5$; light blue: $-1.5 > \log(\rho/\langle \rho \rangle) \geq -2.5$; dark blue: $-2.5 > \log(\rho/\langle \rho \rangle) \geq 0.0$.

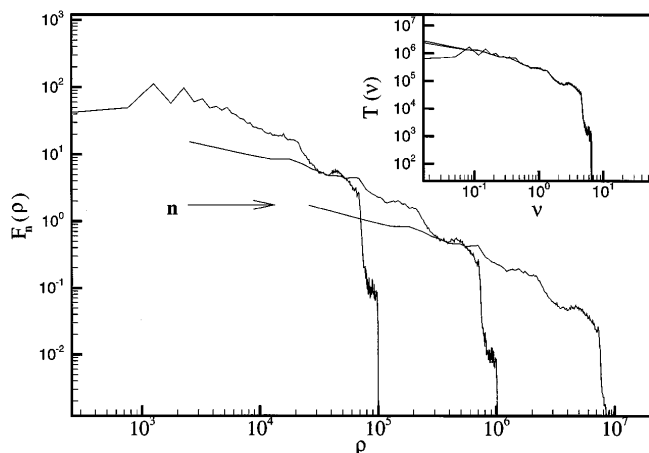


FIG. 3. Main panel: $F_n(\rho)$ for $T = 1.6$, $n = 6-8$. As shown in the inset, a simple scaling makes $F_n(\rho)$ collapse onto a single curve.

Let us consider the rate of growth of the interface (filament length), which is inversely proportional to the rate of decay of length scales in the partially mixed structure. Naively, one would expect the filament length to grow as $L_n \approx e^{\Lambda n}$, where Λ is the Liapunov exponent of the flow. However, numerical results [7,12,16,17] have shown that the filament in fact grows distinctively faster than this prediction. This observation is confirmed in Fig. 4, which shows that the length of the filament L_n actually grows as $L_n \approx e^{\theta n}$, with $\theta > \Lambda$, where θ is also referred to as the topological entropy exponent [16,17,20]. Beigie *et al.* [12] attributed this accelerated growth to the non-Gaussian nature of stretching distributions. In fact, it is due to the nonuniform nature of stretching fields [16] and is observed for a wide range of flows [16,17] regardless of whether the distribution is Gaussian or not (several flows are discussed in Table I). While the exponential factor $e^{\theta n}$ is the *arithmetic* average of

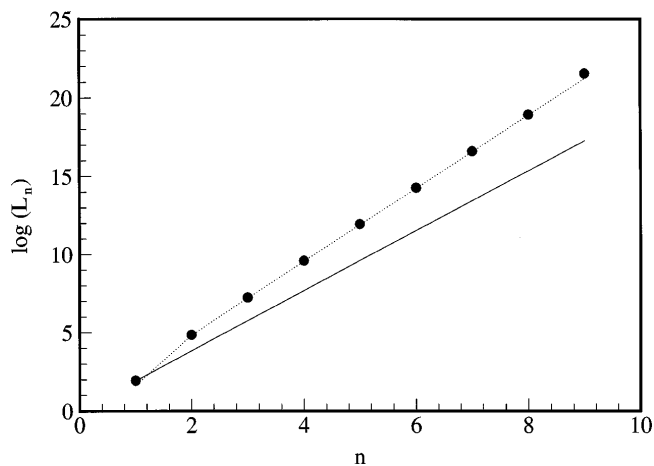


FIG. 4. Comparison of the rate of growth of the filament (●) with the rate of stretching in the flow as predicted by the Liapunov exponent (solid line) for $T = 1.6$.

the stretching experienced by a set of vectors uniformly spaced along the initial filament, i.e.,

$$L_n \approx e^{\theta n} \approx L_0 \langle \lambda_n(x_0(z)) \rangle = \int_0^{L_0} \lambda_n(z) dz, \quad (3)$$

where $z \in [0, L_0]$ parametrizes the initial filament length, the Liapunov exponent is proportional to the *geometric mean* of the stretching. For the sine flow discussed here, we observe $\theta = 1.14$ vs $\Lambda = 0.62$ for $T = 0.8$; $\theta = 1.84$ vs $\Lambda = 1.41$ for $T = 1.2$; $\theta = 2.35$ vs $\Lambda = 1.93$ for $T = 1.6$. These values are independent of the initial location of the filament.

The following procedure is used to compute the distribution of length scales of mixed structures resulting from the advection of a closed filament in an infinite domain: (i) The flow domain is covered with uniformly spaced horizontal lines. (ii) At the end of each period, the intersections of the filament with the lines are computed. (iii) At each intersection, the local angle of the filament relative to the horizontal coordinate is computed. (iv) The local length scales are determined along a line as the distance s between alternating intersections, corrected for the intersection angle. As expected, local length scales span many orders of magnitude; for $T = 1.6$, $n = 5-8$, they have values in the range from 10^{-4} to 10^{-12} . Figure 5 (main panel) shows the frequency distribution $H_n(\log s) = (1/N_s) dN(\log s)/d(\log s)$, where s is a value of the local length scale, N_s is the total number of measurements, and $dN(\log s)$ is the number of values of length scale between $\log s$ and $\log s + d \log s$. For $n \geq 4$, the curves all have the same shape. The same behavior is observed for $T = 0.8$, $n \geq 6$, and for $T = 1.2$, $n \geq 8$ (not shown). In all three cases, curves become almost identical to each other after just a few periods as $H_n(\log s)$ asymptotically approaches a self-similar distribution.

The self-similarity of $H_n(\log s)$ is made explicit by applying a simple rescaling, i.e., $H_n(\log s) = \mathbf{H}(v)$, where $v = [(\log s) - \langle \log s \rangle] / \sigma_{\log s}$. The only parameters required in this scaling are $\langle \log s \rangle$ and $\sigma_{\log s}$. For an area-preserving flow such as the one considered here, the mean of $\log s$ evolves as $\langle \log s \rangle = -n\theta$. The standard deviation also increases linearly in time, i.e., $\sigma_{\log s} \approx nK$, where K is a constant particular for each T value. Therefore, v can be expressed in terms of n , i.e., $v \approx (\log s + n\theta)/nK$. As shown in Fig. 5 (inset), when rescaled in this manner, $H_n(\log s)$ asymptotically collapses onto a time-invariant curve, highlighting the importance of properly predicting the exponent θ .

In conclusion, several observations can be made: (i) Time-periodic flows create mixing structures that are self-similar in time; (ii) filaments grow at an exponential rate (dictated by the topological entropy exponent) that is significantly greater than predicted by the Liapunov exponent; (iii) filament density is strongly nonuniform, and is characterized by a self-similar frequency distribution;

TABLE I. The table shows values of θ and Λ for multiple parameter values for the sine flow (the main case study considered in this paper); for a classic map from the literature, the standard map; for a physically realizable 2D flow (the periodicity driven cavity flow [18]); for the industrially relevant 3D Kenics mixer [19]).

Sine flow			Standard map			Cavity flow			Kinetic mixer		
T	θ	Λ	T	θ	Λ	T	θ	Λ	Re	θ	Λ
0.80	1.14	0.62	0.80	2.41	2.08	5.00	0.88	0.61	1.00	9.71	1.54
1.00	1.48	1.12	1.20	2.74	2.44	5.60	1.22	0.80	10.00	7.77	1.55
1.20	1.84	1.41	1.60	3.00	2.77	6.00	1.19	0.85	100.00	1.16	0.80
1.40	2.12	1.72	2.00	3.25	2.99	7.00	1.77	0.83	1000.00	2.47	1.19
1.60	2.35	1.93	2.40	3.41	3.17	8.00	3.35	1.15			
1.80	2.54	2.14				9.00	4.12	1.29			
2.00	2.78	2.34				10.00	5.18	1.45			

(iv) the length scale distribution generated by the flow is also self-similar.

These observations have important practical implications: (i) Predictions of an average “striation thickness” based on the Liapunov exponent would be inaccurate. (ii) Mixing in some regions of a time-periodic chaotic flow is much more intimate than in other regions. The observed nonuniformities in filament density mean that time-periodic flows wastefully concentrate most of their mixing action in narrow subregions of the flow that are already well mixed. For systems in which the rate of reaction depends directly on the creation of intermaterial surface between the reacting fluids, such reactions would be much faster in regions that are densely populated by the filament. (iii) For systems with multiple competing reactions, this nonuniformity means that different reaction rates and product distributions would be observed in various locations. Accurate knowledge of the evolution of the striation thickness distribution as it approaches the self-similar state could greatly facilitate the development of useful models of reactive laminar flows.

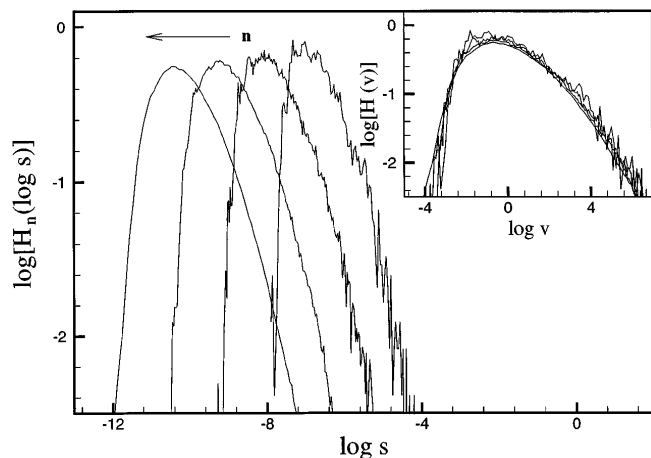


FIG. 5. Main panel: $H_n(\log s)$, for $T = 1.6, n = 5-8$. As shown in the inset, a simple scaling makes $H_n(\log s)$ collapse onto a single curve.

*Author to whom correspondence should be addressed.

- [1] C. W. Leong and J. M. Ottino, *J. Fluid Mech.* **209**, 463 (1989).
- [2] C. W. Leong, Ph.D. Dissertation, University of Massachusetts, 1990.
- [3] D. J. Lamberto, F. J. Muzzio, and P. D. Swanson, *Chem. Eng. Sci.* **51**(5), 733 (1996).
- [4] P. D. Swanson and J. M. Ottino, *J. Fluid Mech.* **213**, 227 (1990).
- [5] F. J. Muzzio and J. M. Ottino, *Phys. Rev. A* **42**, 5873 (1990).
- [6] B. J. Bayly and S. Childress, *Phys. Rev. Lett.* **59**, 1573 (1987).
- [7] J. M. Finn and E. Ott, *Phys. Fluids* **31**, 2992 (1988).
- [8] A. M. Soward and B. J. Bayly, in *Lectures on Solar and Planetary Dynamos*, edited by M. R. E. Proctor and A. D. Gilbert (Cambridge University Press, Cambridge, England, 1994).
- [9] S. Childress and A. D. Gilbert, *Stretch, Twist, and Fold: The Fast Dynamo* (Springer-Verlag, Berlin, 1995).
- [10] H. Aref, *J. Fluid Mech.* **143**, 1 (1984); D. V. Khakhar, H. Rising, and J. M. Ottino, *J. Fluid Mech.* **172**, 419 (1986); V. Rom-Kedar, A. Leonard, and S. Wiggins, *J. Fluid Mech.* **214**, 347 (1991).
- [11] P. Tanga and A. Provenzale, *Physica (Amsterdam)* **76D**, 202 (1994).
- [12] D. Beigie, A. Leonard, and S. Wiggins, *Phys. Rev. Lett.* **70**, 275 (1993).
- [13] F. J. Muzzio, P. D. Swanson, and J. M. Ottino, *Phys. Fluids A* **3**, 822 (1991).
- [14] J. G. Franjione and J. M. Ottino, *Phys. Fluids* **12**, 3641 (1987).
- [15] J. C. H. Fung and J. C. Vassilicos, *Phys. Fluids A* **3**, 2725 (1991).
- [16] E. M. Ziemniak, C. Jun, and T. Tél, *Physica (Amsterdam)* **76D**, 123 (1994).
- [17] Z. Neufeld and T. Tél, *J. Phys. A* **30**, 2263 (1997).
- [18] M. Liu, F. J. Muzzio, and R. L. Peskin, *Chaos Solitons Fractals* **4**, 2145 (1994).
- [19] D. M. Hobbs, M. M. Alvarez, and F. J. Muzzio, *Fractals* **5**(3), 395 (1997).
- [20] J. P. Eckmann and D. Ruelle, *Rev. Mod. Phys.* **57**(3), 617 (1985).